











Precision measurements of the ${}^2P_{1/2}$ - ${}^2P_{3/2}$ fine-structure splitting in B-like S^{11+} and Cl^{12+} X. Liu ^{1,2}, X. P. Zhou,¹ W. Q. Wen ^{1,3,*}, Q. F. Lu,⁴ C. L. Yan,⁴ G. Q. Xu ⁴, J. Xiao ^{4,*}, A. V. Volotka ⁵,
Y. S. Kozhedub ⁶, M. Y. Kaygorodov,⁶ Z. K. Huang ^{1,3}, W. L. Ma ⁷, S. X. Wang ⁷ and X. Ma ^{1,3}¹*Institute of Modern Physics, Chinese Academy of Sciences, 730000 Lanzhou, China*²*Guangdong Provincial Key Laboratory of Nuclear Science, Institute of Quantum Matter, South China Normal University, Guangzhou 510006, China*³*University of Chinese Academy of Sciences, 100049 Beijing, China*⁴*Shanghai EBIT Laboratory, Key Laboratory of Nuclear Physics and Ion-Beam Application (MOE), Institute of Modern Physics, Fudan University, Shanghai 200433, China*⁵*School of Physics and Engineering, ITMO University, Kronverkskiy prospekt 49, 197101 St. Petersburg, Russia*⁶*Department of Physics, St. Petersburg State University, Universitetskaya 7/9, 199034 St. Petersburg, Russia*⁷*Department of Modern Physics, University of Science and Technology of China, 230026 Hefei, China*

(Received 19 October 2021; accepted 18 November 2021; published 8 December 2021)

The fine-structure splitting $1s^2 2s^2 2p \ {}^2P_{1/2}$ - ${}^2P_{3/2}$ transitions in boronlike S^{11+} and Cl^{12+} were experimentally measured with a high precision spectrometer at the Shanghai high-temperature superconducting electron beam ion trap. The $M1$ transition wavelengths for S^{11+} and Cl^{12+} were determined to be 760.9635(29) and 574.1539(26) nm (in air), respectively. Compared to the previously observed results, the accuracies of current experimental results are improved by more than ten times and 200 times for S^{11+} and Cl^{12+} , respectively. Additionally, the $M1$ transition energies in S^{11+} and Cl^{12+} were evaluated within the *ab initio* QED framework to compare with the experimental data. The present experimental results agree with the theoretical calculations and provide a possibility to test QED effects and correlation effects with high accuracy in few-electron highly charged ions.

DOI: [10.1103/PhysRevA.104.062804](https://doi.org/10.1103/PhysRevA.104.062804)**I. INTRODUCTION**

Precision measurements of the fine-structure splitting of highly charged ions (HCIs) test fundamental atomic theory, including strong field quantum electrodynamics (QED) effects, electron correlation effects, and relativistic and nuclear effects [1–8]. The magnetic dipole ($M1$) transitions of $1s^2 2s^2 2p \ {}^2P_{1/2}$ - ${}^2P_{3/2}$ in boronlike HCIs are the origin of many solar coronal lines and thus of great interest in determining the properties of astrophysical as well as fusion plasmas [9–13]. Furthermore, since the ${}^2P_{1/2}$ and ${}^2P_{3/2}$ levels of boronlike systems are degenerate within the framework of the nonrelativistic theory [14–17], the transition energy of fine-structure splitting is completely determined by the relativistic and QED effects [5,18]. Therefore, precision measurements of these transition wavelengths as well as the transition rates allow us to investigate the electron correlation, relativistic, and QED corrections up to an extremely high level of accuracy [4,19,20]. In addition, the ${}^2P_{1/2}$ - ${}^2P_{3/2}$ fine-structure splitting of boronlike ions are also considered as the basis for extremely accurate HCI optical clocks with precision laser techniques, since these $M1$ transitions of intermediate nuclear charge Z lie in the optical regime of the spectra and have small radiative

widths with the lifetime of the $P_{3/2}$ level being of order ms [21–25].

For experimental spectroscopy of boronlike HCIs, the $M1$ transition wavelengths of boron isoelectronic sequence were provided by the astronomical observation and compared with the calculations by Edlén in 1983 [26]. The observation accuracies are generally not high. In order to obtain a more accurate spectrum of the boronlike ions, the heavy-ion storage rings and electron beam ion traps (EBITs) are employed to carry out precision measurements of the spectroscopy for HCIs. High precision measurements of the $M1$ fine-structure transitions in highly charged boronlike argon, which lie in the visible region of the spectrum, were performed at the Oxford EBIT with uncertainties of 7 ppm [27]. Afterwards, the transition probabilities of the $M1$ transition ${}^2P_{1/2}$ - ${}^2P_{3/2}$ in several boronlike ions have been measured using the Heidelberg heavy-ion storage ring TSR and the Livermore electron-beam ion trap EBIT-I [3,14,28]. In 2003, Draganić *et al.* reported a high precision measurement of the $M1$ transition energy in boronlike Ar^{13+} using the Heidelberg EBIT, where the experimental precision is 200 times better than previous measurements and shows great potential for the study of QED effects in relativistic few-electron HCIs systems [4]. In addition, the lifetime of the $Ar^{13+} \ 1s^2 2s^2 2p \ {}^2P_{3/2}$ metastable level and isotope shifts of boronlike ${}^{36,40}Ar^{13+}$ were determined with sub-ppm accuracy at the Heidelberg EBIT to investigate the relativistic electron correlation, QED, and nuclear recoil effects [29,30]. In 2011, Mäckel *et al.* demonstrated

*Corresponding authors: wenweiqiang@impcas.ac.cn; xiao_jun@fudan.edu.cn

the resonant fluorescence laser spectroscopy of the dipole-forbidden $1s^2 2s^2 2p^2 P_{1/2} - ^2P_{3/2}$ transition in boronlike Ar¹³⁺ ions stored in an EBIT [31], and the measured *M1* transition wavelength was 441.255 68(26) nm. Very recently, there have been ongoing efforts to significantly increase the experimental accuracy by employing the charged particle Penning traps and Paul traps, which allow one to slow the ion motion nearly to rest, thus reducing Doppler effects and increasing the possible accuracy to the ppb level [22,25,32]. In addition to the experimental efforts, a number of theoretical calculations of the transition energies and rates for boronlike ions have already been reported previously to understand the roles of electron correlation and relativistic effects as well as the QED effects [18,19,24,33,34]. Until now, the most accurate theoretical prediction for the $1s^2 2s^2 2p^2 P_{1/2} - ^2P_{3/2}$ transition energies in boronlike ions have been obtained within the *ab initio* QED framework [5,19].

Here, we present the precision measurements of the $^2P_{1/2} - ^2P_{3/2}$ fine-structure splitting in boronlike S¹¹⁺ and Cl¹²⁺ ions at the Shanghai high-temperature superconducting electron beam ion trap (SH-HtscEBIT). These measurements are supported by the theoretical calculations performed with the *ab initio* QED approach in the extended Furry picture. Comparison between experimental and theoretical results reveals an excellent agreement. *Ab initio* theoretical calculations of these transitions with $^2P_{1/2} - ^2P_{3/2}$ were also done. The results of the calculations, which have a larger uncertainty than the experiment, were found to be in good agreement.

The paper is organized as follows: Section II presents the experimental method, which shows the details of the SH-HtscEBIT and the calibration system. In Sec. III, the theoretical method and the results of the calculations of the *M1* transition wavelengths are reported. Section IV presents the detailed analysis of the experimental results and the comparison with previous results from the literature. Finally, we summarize the results as a conclusion in Sec. V.

II. EXPERIMENTAL METHOD

The present experiments of precision spectroscopy with highly charged boronlike S¹¹⁺ and Cl¹²⁺ ions were performed at the SH-HtscEBIT [35–38]. The details about precision spectroscopy experiments with HCIs at the SH-HtscEBIT can be found in Ref. [35] and references therein. Here, we only briefly describe the precision measurements of the fine-structure splitting in boronlike S¹¹⁺ and Cl¹²⁺. The electron beam emitted from the hot cathode electron gun was accelerated by the high voltage between the drift tubes and the electron gun and reached the target energy when entering the drift tubes. At the same time, the electron beam was magnetically focused by the high-temperature superconducting coils, which were radially surrounded outside the drift tubes. Thus, the electron beam diameter was compressed to $\sim 150 \mu\text{m}$ by a magnetic field of 0.2 T. In order to produce boronlike S¹¹⁺ and Cl¹²⁺ ions, the gases of SF₆ and CCl₄ were continuously injected into the EBIT through the gas injection system. The background vacuum pressure at the EBIT center was less than 1.0×10^{-9} Torr, and gas injection pressures were controlled at 1.0×10^{-7} Torr, which increases the probabilities of electron impact ionizations to produce the target ions.

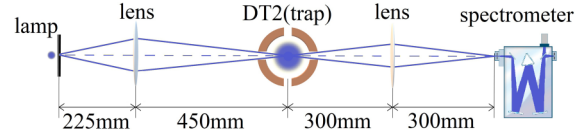


FIG. 1. Schematic diagram of calibration scheme for the spectrometer to be measured at the SH-HtscEBIT. The HCIs are trapped at the center of DT2 in the EBIT.

The visible spectra were observed and analyzed using the Czerny-Turner spectrometer (Andor Shamrock-303i), connected to one of the viewports at the SH-HtscEBIT. A 1200-L/mm grating (Blaze wavelength: 500 nm) was used to disperse the photons from the ion deexcitation in the drift tube, and the photons were then detected by the charge-coupled device (CCD) detector (ANDOR DU971P-UVB). The present visible range spectrometer covers a spectral range from 200 to 800 nm. In order to calibrate the observed emission spectra from S¹¹⁺ and Cl¹²⁺ ions, which are trapped at the center of drift tube 2 (DT2), a new conjugate calibration system was constructed, and the schematic view is shown in Fig. 1. To obtain a larger collection solid angle, a biconvex lens with a focal length of $f = 150$ mm is placed between the window and the entrance slit of the spectrometer ($30 \mu\text{m}$). A convex lens $f = 150$ mm was used to the left of EBIT to make the calibration light source into a real image in the center of the well region of EBIT, so that the position of the calibration light source was coincident with the ion position in EBIT. It should be noted that the image distance and object distance in the figure are calculated by the lens imaging formula to ensure the overlap of the calibration light source and the emission light source at the same position inside the trap [39].

The emission spectra of S¹¹⁺ and Cl¹²⁺ were recorded under different nominal electron beam energies. The exposure time was typically 1–2 h for each spectrum measurement. In order to increase the signal-to-noise ratio, the spectra were accumulated for a longer time under the electron beam energy with the strongest observed peak. The background measurements were performed under the condition with electron beam off, but with the cathode still heated, to distinguish the emission spectra from the background structure of the stray light from the cathode. The measured wavelengths of S¹¹⁺ ions were calibrated using external Kr and Ar lamps, and the measured wavelengths of Cl¹²⁺ ions were calibrated using external Hg, Kr, and Ne lamps, respectively. As shown in Table I, the reference wavelengths of the calibration lines used in the spectrum calibration process come from the Ritz wavelength (in air) in the NIST database [40]. In order to

TABLE I. Wavelengths (in air) of the calibration lines [40].

Ions	Element	Wavelength (nm)
S ¹¹⁺	Kr	758.741 34, 760.154 54, 768.524 58, 769.453 99
	Ar	727.2935, 738.3980, 750.3868, 751.4651, 763.5105
Cl ¹²⁺	Hg	546.074 98
	Kr	556.222 53, 557.028 93, 587.091 57
	Ne	585.248 79, 594.483 42

reduce the effect of possible long-term mechanical drifts of the setup, individual calibrations were carried out before and after each measurement of the S and Cl emission lines. It should be mentioned here that all the wavelengths measured in the present experiment are indexed by air wavelength, and the details for conversion between air and vacuum wavelengths can be found in Ref. [41].

III. THEORY

The most accurate theoretical prediction for the $1s^2 2s^2 2p^2 P_{1/2-2} P_{3/2}$ transition energies in boronlike S^{11+} and Cl^{12+} ions can be obtained within the *ab initio* QED framework [5,19,42,43]. The starting point of such calculations is extended with the Furry picture of QED, which is based on the solutions of the Dirac equation with an effective potential. An effective potential includes both the Coulomb potential of the nucleus and the mean-field potential created by electrons V^{scr} . In the present calculations, for the screening potential we use so-called core Hartree (CH),

$$V^{\text{CH}}(r) = \alpha \int_0^\infty \frac{\rho^c(r')}{\max(r, r')} dr', \quad (1)$$

and Kohn-Sham (KS),

$$V^{\text{KS}}(r) = \alpha \int_0^\infty \frac{\rho^t(r')}{\max(r, r')} dr' - \frac{2\alpha}{3r} \left[\frac{81}{32\pi^2} r \rho^t(r) \right], \quad (2)$$

potentials. The core-Hartree potential arises from the charge distribution ρ^c of the core electrons, $1s^2 2s^2$, while the Kohn-Sham potential also includes the exchange-type of interaction between valence and core electrons. The total charge distribution ρ^t is constructed for the ground state configuration of the boronlike ion. Solving the Dirac equation with such a potential, one gets the zero-order result, the so-called Dirac value. Further, we develop the bound-state QED perturbation theory for the interaction Hamiltonian density,

$$h^{\text{int}}(t, \mathbf{r}) = e\alpha^\mu A_\mu(t, \mathbf{r}) - V^{\text{scr}}(r), \quad (3)$$

where α^μ are the Dirac matrices and A_μ is the quantized electromagnetic field. In the first order, we get the following contributions: one-photon exchange and one-loop radiative [self-energy (SE) and vacuum polarization (VP)] diagrams. These diagrams are computed employing the well-known formal expressions, which can be found in Refs. [44,45]. In the second order, we get a two-photon exchange, screened radiative, and two-loop radiative diagrams. The first two sets of diagrams are rigorously evaluated, employing the techniques and methods presented in detail in Refs. [46–49]. Here, however, in contrast to the previous *ab initio* calculations of boronlike ions [5,19,42,43], we include in addition higher-order screened radiative contributions evaluated within the model operator approach [50]. The contribution from the two-loop diagrams has been estimated using the hydrogenic values given in Ref. [51]. Next, one has to consider the third-order contributions. However, the corresponding diagrams are much too complicated for the rigorous calculations and, so far, cannot be accessed via the *ab initio* QED treatment. Despite this, we have to account for the higher-order correlation correction for the transitions under consideration. In order to take this

into account, we apply the Breit approximation and utilize the configuration-interaction Dirac-Fock-Sturm (CIDFS) method [52–54]. In this method, the many-electron wave function Ψ and the energy of an atom E within the Breit approximation are to be found as solutions of the Dirac-Coulomb-Breit Hamiltonian H^{DCB} [55,56],

$$(\Lambda^+ H^{\text{DCB}} \Lambda^+) \Psi = E \Psi, \quad (4)$$

where Λ^+ is a projector operator, which is discussed below. The eigenvalue problem is solved in the many-electron basis of configuration state functions (CSFs), with each CSF being an eigenfunction of the J^2 operator. The Hamiltonian H^{DCB} is given by a sum over all electrons of the one-electron Dirac Hamiltonians h_i^{D} and two-electron Coulomb V_{ij}^{C} and Breit V_{ij}^{B} interactions,

$$H^{\text{DCB}} = \sum_i h_i^{\text{D}} + \sum_{i<j} (V_{ij}^{\text{C}} + V_{ij}^{\text{B}}). \quad (5)$$

The many-electron basis is spanned by the eigenfunctions of the h^{D} Hamiltonian represented in the combined basis of the Dirac and Dirac-Sturm orbitals. The Λ^+ projectors in Eq. (4) are the product of one-electron projectors on the positive energy-states of h^{D} Hamiltonian. In the present work, the Dirac Hamiltonian h^{D} includes also the screening potential V^{scr} to fix the Λ^+ projectors in a consistent way with the rigorous QED calculations [19].

In Table II, we present the individual theoretical contributions to the fine-structure transition energies in boronlike S^{11+} and Cl^{12+} ions calculated as has been explained above. In addition to the contributions obtained within the Furry picture of QED, we include also the nuclear recoil correction, which has been evaluated similarly as in Refs. [46,57]. In order to calculate the ground state transition energies of boronlike S^{11+} and Cl^{12+} more accurately, we used two different initial approximations based on the CH and KS screening potentials. The calculated results are shown in Table II, which includes two sets of results with different potentials for each ion. The contributions are divided into the zeroth-order Dirac term, the correlation corrections (first, second, and higher orders) evaluated within the Breit approximation, the first- and second-order QED effects, and the recoil term. As one can see from the table, the total results based on the two different initial approximations (CH and KS) perfectly agree with each other, thus, demonstrating the consistency of the calculation. The uncertainties of the total theoretical values are determined by the basis size in the CIDFS calculation [term correlation, (3+)] as well as by the QED two-loop diagrams, which are accounted here only approximately [term QED, (2)]. As can be seen from Table II, the QED contributions in boronlike S^{11+} and Cl^{12+} ions both reached 0.2% of the transition energy. In Table II, we also present the results of another *ab initio* calculation, Ref. [19], performed with the core-Hartree potential for the case of Cl^{12+} ion. Comparing the individual terms with those of Ref. [19], one identifies three contributions, the first-order correlation (1) as well as the first- and second-order QED (1) and (2), that disagree considerably with each other. Concerning the correlation (1) and QED (1) terms, we notice that its sum [correlation (1) + QED (1)] gives -0.09593 eV for our calculations and -0.0959 eV for calculations of Ref. [19]. This perfect agreement means that

TABLE II. Individual contributions to the ground state $M1$ transition energies in boronlike S^{11+} and Cl^{12+} ions (in eV). The zeroth-order Dirac result is extended by the correlation corrections evaluated within the Breit approximation, by the first- and second-order QED contributions, as well as by the recoil term. Calculations were performed employing two starting potentials, core-Hartree and Kohn-Sham. The final results appeared to be independent of the initial potential are given in the last row. For comparison, in the fifth column, the individual contributions obtained in Ref. [19] within the core-Hartree potential for Cl^{12+} ion are displayed.

Contributions	S^{11+}		Cl^{12+}		
	Core-Hartree	Kohn-Sham	Core-Hartree	Core-Hartree [19]	Kohn-Sham
Dirac	1.763 01	1.795 81	2.327 60	2.3276	2.368 27
Correlation (1)	−0.08 043	−0.112 81	−0.100 34	−0.1011	−0.140 69
Correlation (2)	−0.110 63	−0.085 68	−0.141 08	−0.1410	−0.108 25
Correlation (3)	0.0538(2)	0.0285(2)	0.0687(2)	0.0686	0.0356(2)
QED (1)	0.00340	0.00343	0.00441	0.0052	0.004 48
QED (2)	−0.0003(3)	−0.0003(3)	−0.0003(3)	0.0003	−0.0004(3)
Recoil	−0.000 09	−0.000 09	−0.000 09	−0.0001	−0.000 08
Total	1.6289(4)	1.6289(4)	2.1589(4)	2.1595	2.1589(4)

individual contributions, correlation (1) and QED (1), might deviate due to the different ways of separating these terms. When we separate the non-Breit, frequency-dependent part of the one-photon exchange diagram, which belongs in our calculations to the QED (1) term, and add it to the correlation (1) correction, our individual terms start to agree with corresponding terms of Ref. [19]. As for the QED (2) term, we notice that in contrast to Ref. [19], we also include the higher-order screened radiative contribution in the present calculations, which gives -0.0004 eV for the Cl^{12+} ion. This contribution largely explains the difference between our and Ref. [19] QED (2) and total values.

IV. RESULTS AND DISCUSSION

The spectra of the boronlike $^{32}S^{11+}$ ion in the visible range 737–77 nm obtained at the nominal electron beam energies of 480, 530, 570, 620, and 690 eV are shown in Fig. 2(a). The accumulation time of each spectrum was 2 h. As can be seen from Fig. 2(a), when the nominal electron beam energy reaches 530 eV, a peak appears at around 760 nm. The intensity of the peak becomes higher and higher with the increase of the electron beam energy, and then the intensity decreases and disappears at 620 eV. According to the NIST database [40], the ionization energies of S^{10+} and S^{11+} are 504.55 and 564.41 eV, respectively. This shows that the line in Fig. 2(a) is consistent with the $^2P_{1/2}-^2P_{3/2}$ $M1$ transition of the S^{11+} ion. When the nominal electron beam energy exceeds the ionization energy of the S^{11+} ion, the S^{11+} ion begins to be ionized, so the peak strength at 760 nm will be weakened. The spectra of boronlike $^{35,37}Cl^{12+}$ ions in the visible range of 541–584 nm obtained at the nominal electron beam energies of 600, 630, 660, 700, 750, and 800 eV are shown in Fig. 2(d). As can be seen from Fig. 2(d), when the energy of the nominal electron beam reaches 630 eV, just exceeding the ionization energy of Cl^{12+} ion, a peak appears at 574 nm, indicating that the line in Fig. 2(d) comes from the $^2P_{1/2}-^2P_{3/2}$ $M1$ transition of boronlike Cl^{12+} ion. In order to improve the signal-to-noise ratio of the obtained spectra, a total accumulation time of 8 h was made under the nominal electron beam energy of 570 eV at the highest spectral peak intensity of S^{11+} ions. Similarly, a total accumulation time of 8 h was made under

the nominal electron beam energy of 700 eV for Cl^{12+} ions. Figures 2(b) and 2(e) are the Gaussian fittings of the strongest peaks of the spectra for S^{11+} and Cl^{12+} ; Figs. 2(c) and 2(f) are the residuals of Gaussian fitting for (b) and (e), respectively. It should be noted that the element of sulfur has only one natural isotope of ^{32}S and the spin of the nucleus is zero, therefore, the spectrum of B-like $^{32}S^{11+}$ has no hyperfine splitting. However, for chlorine, the naturally occurring isotopes include ^{35}Cl and ^{37}Cl with the abundance of 75.8% and 24.2% and the spin of these two isotopes is 3/2. As a result, the precision spectrum of $^{35,37}Cl^{12+}$ includes the isotope shift and also the hyperfine splitting effects. The isotope shifts for the $^2P_{1/2}-^2P_{3/2}$ transition in boronlike $^{35,37}Cl^{12+}$ is about 0.0032 meV [58], which is much smaller than the current experimental accuracy with 0.010 meV. For $^{35}Cl^{12+}$ and $^{37}Cl^{12+}$ the hyperfine splitting of the ground state is 0.044 and 0.037 nm, respectively. Since the asymmetric line broadening caused by hyperfine splitting as well as the isotope shift effect is very tiny, the fitted line center has a very high accuracy of 0.04 pm. Therefore, the influence of isotope shift and hyperfine splitting effects can be safely neglected in the present experimental measurement.

The uncertainty of the determined transition wavelengths at the EBIT mainly comes from the uncertainty in determining the center of the line, the dispersion function, the calibration lines, and the calibration system [59]. We will describe the detailed analysis of error sources below.

Line centroid uncertainty. The uncertainty of the center of the line is mainly caused by the finite signal-to-noise ratio of the measured spectrum. The centers of the emission lines are determined by fitting the spectra with Gaussian functions. We checked that the observed line shape was correctly described by a single Gaussian, by verifying that there was no significant structure in the residuals, and that there was no significant dependence of the centroid on the fit interval. In order to reduce the statistical errors, the spectra of S^{11+} and Cl^{12+} ions have been measured multiple times (24 times for S^{11+} , 52 times for Cl^{12+}), and the resulting centroids are shown in Fig. 3. The results of multiple measurements are weighted and averaged according to the uncertainty of the fitting (for the individual centroids weighted as $1/\sigma^2$, σ is the uncertainty of

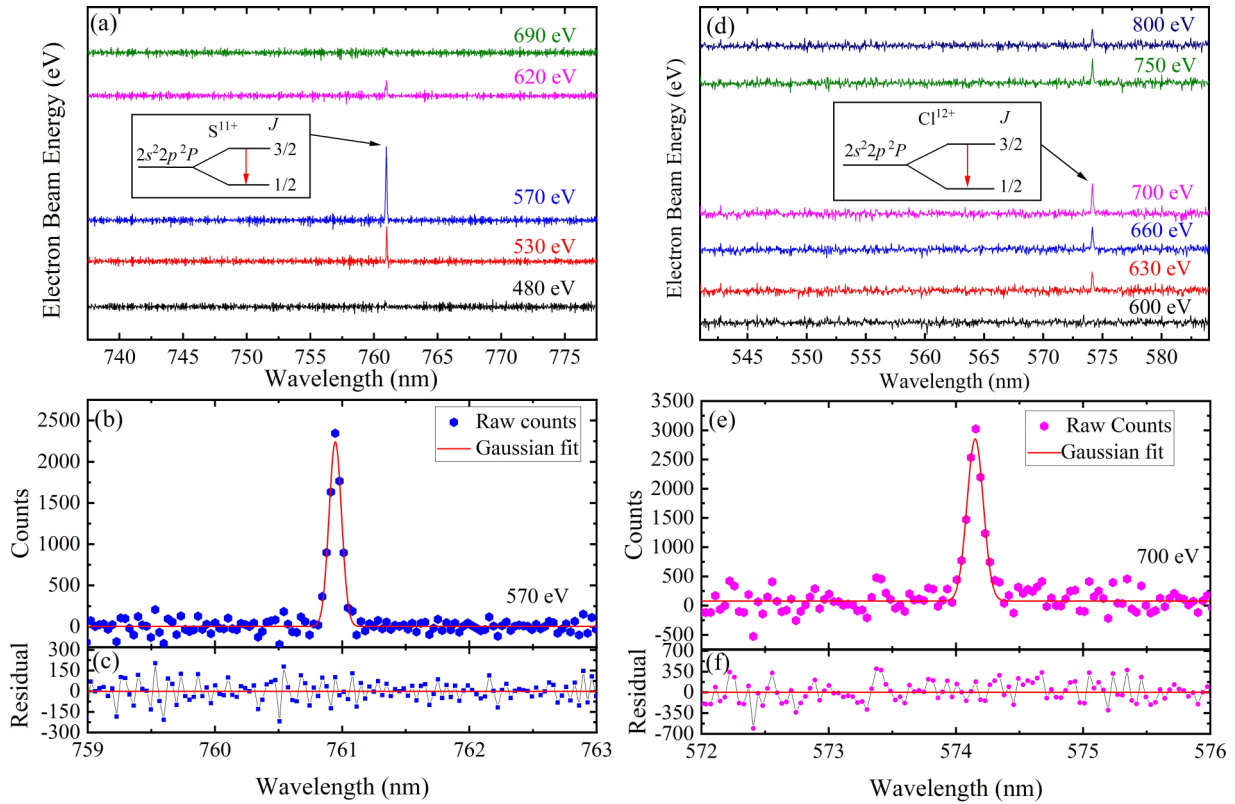


FIG. 2. (a) Spectra of sulfur obtained at the SH-HtscEBIT with nominal electron beam energies of 480, 530, 570, 620, and 690 eV in the range 737–777 nm. The line is the $M1$ transition between the fine-structure levels in the $2s^2 2p^2 P$ ground term of boronlike S^{11+} . (b) Expanded view of the line at 761 nm and its Gaussian fit. (c) Residuals of Gaussian fitting for S^{11+} . (d) Spectra of chlorine with nominal electron beam energies of 600, 630, 660, 700, 750, and 800 eV. The line is the $M1$ transition between the fine-structure levels in the $2s^2 2p^2 P$ ground term of boronlike Cl^{12+} . (e) Expanded view of the line at 571 nm and its Gaussian fit. (f) Residuals of Gaussian fitting for Cl^{12+} .

each centroid obtained in the fit), and the weighted average measurement wavelengths are 760.9635 ± 0.0007 nm and 574.1539 ± 0.0003 nm for S^{11+} and Cl^{12+} , respectively.

Dispersion function uncertainty. The uncertainty of the dispersion function mainly comes from the Gaussian fitting of the calibration line and the statistical uncertainty of the dispersion function using the second or third polynomial fitting. As shown in Figs. 4(a) and 4(d), the measured wavelengths of

S^{11+} ions were calibrated using the external Kr and Ar lamps, while the measured wavelengths of Cl^{12+} ions were calibrated using the external Hg, Kr, and Ne lamps. Figures 4(b) and 4(e) show the deviations from the dispersion function fitted by the first-, second-, and third-order polynomial functions for S^{11+} and Cl^{12+} , respectively. The uncertainty of the dispersion function caused by the fitting is evaluated by calculating the standard deviation of the residual error of the polynomial

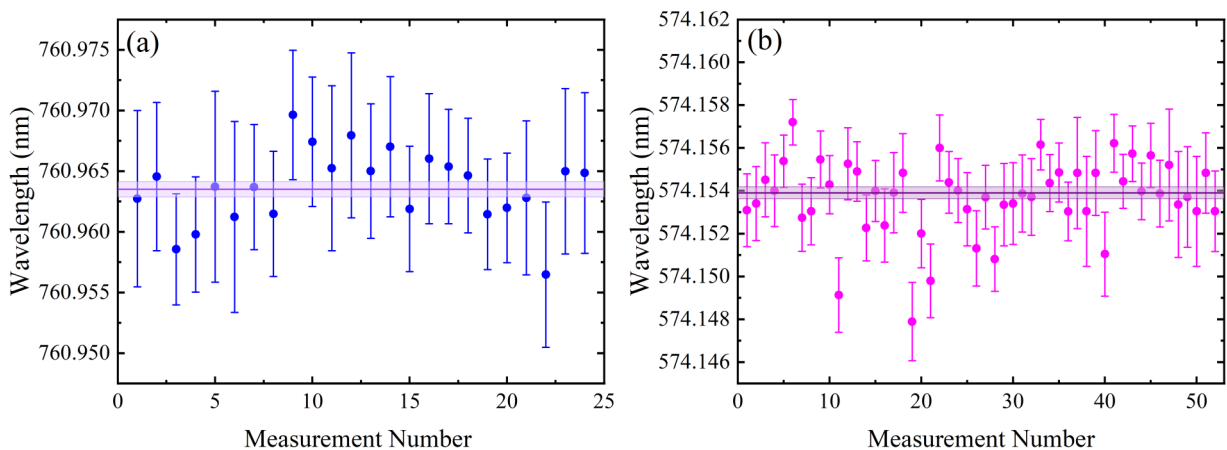


FIG. 3. Multiple measurement results of $M1$ transition wavelength, (a) for S^{11+} ions and (b) for Cl^{12+} ions. The dark line in the figure represents the weighted average wavelength, and the light-colored band represents the uncertainty of the weighted average wavelength.

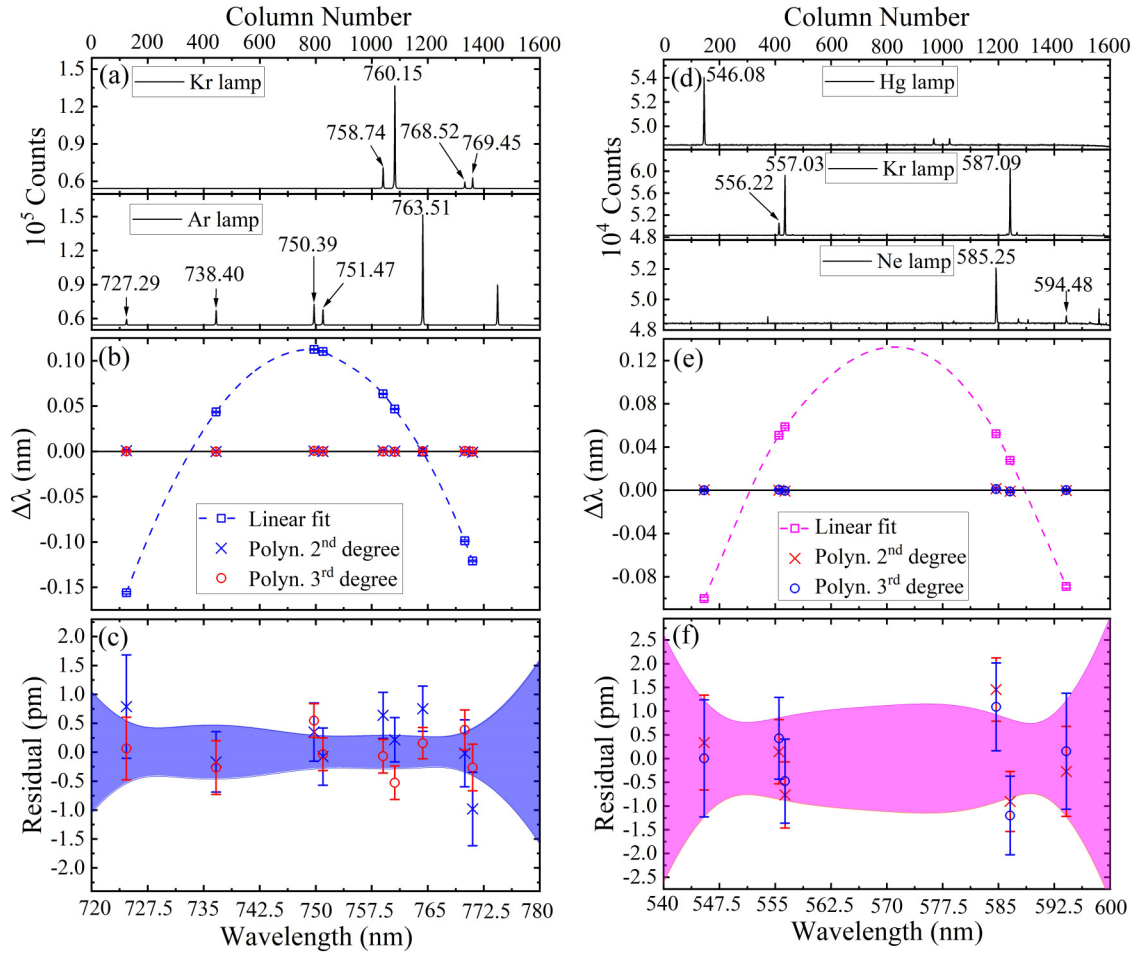


FIG. 4. (a) Spectrum of Kr and Ar lamp calibration lines for S^{11+} ions. (b) All residuals from the dispersion function fit, using first (square), second (cross), and third (circle) degree polynomials for the dispersion function. (c) Second and third degree polynomial residuals (enlarged scale), the light-colored band is a $1-\sigma$ confidence band for S^{11+} ions. (d) The spectrum of Hg, Kr, and Ne lamp calibration lines for Cl^{12+} ions. (e) All residuals from the dispersion function fit, using first (square), second (cross), and third (circle) degree polynomials for the dispersion function of Cl^{12+} ions. (f) Second and third degree polynomial residuals (enlarged scale), the light-colored band is a $1-\sigma$ confidence band for Cl^{12+} ions.

fitted by the dispersion function. The uncertainties of the dispersion function of the multiple measurements are averaged in the experiments. Figures 4(c) and 4(e) show the second- and third-degree polynomial residuals for S^{11+} and Cl^{12+} ions, and the light-colored band is a $1-\sigma$ confidence band. Since the emission spectra for S^{11+} and Cl^{12+} have been measured and calibrated for 24 and 52 times, finally, the uncertainties of the dispersion functions in the spectra measurements are 0.76 and 0.64 pm for S^{11+} and Cl^{12+} ions, respectively.

Calibration lines uncertainty. The uncertainties due to the calibration lines are mainly due to the uncertainties of the wavelengths of the calibration lines. In principle, the wavelength accuracies of the calibration lines are very high, and the resulting uncertainties can be ignored. However, to be conservative in the present experiment, the uncertainties of the calibration lines were all less than or equal to 0.1 pm for S and 0.05 pm for Cl. For simplicity we use 0.1 and 0.05 pm as systematic uncertainties due to the calibration lines for S and Cl respectively.

Calibration systematic uncertainty. An important systematic result is from the nonequivalence of the spatial and angular distribution of the light from the EBIT and the calibration lamps. In this work, the uncertainty of the calibration system was evaluated by alternately measuring the Ne I 585.24-nm atomic line by injection of Ne into the EBIT and the 585.24-nm spectral line of the standard calibration Ne lamp. We fit the lines of Ne I 585.24 nm from the EBIT and from the calibration line as before, and the obtained wavelength shift is 1.76 pm. In addition, the fine-structure splitting $1s^2 2s^2 2p^2 P_{1/2} - ^2P_{3/2}$ transition of boronlike Ar^{13+} was measured in the air, i.e., 441.2567(26) nm, which is 0.8 pm as compared with the very precise results in Ref. [32]. So, we take the larger of these two shifts, 1.76 ppm, to be a good estimate of the uncertainty due to the calibration system.

Other uncertainties. In this work, the line center wavelength shift caused by the space charge Stark effect of the electron beam and the wavelength shift caused by the collisions are negligible under the current measurement accuracy. In addition, in the center of the drift tube, the magnetic field

TABLE III. Uncertainties of the measured wavelengths.

Source	Uncertainty in wavelength (10^{-3} nm)	
	S^{11+}	Cl^{12+}
Ions		
Line centroid	0.7	0.3
Dispersion function	0.76	0.64
Calibration lines	0.1	0.05
Calibration systematic	1.76	1.76
Total	2.9	2.6

strength reaches 0.16 T, which will cause the Zeeman split of the spectral line. However, the Zeeman effect in the current magnetic field is extremely weak. The estimated Zeeman splittings are 0.007 and 0.004 nm which are much smaller than the observed linewidths of 0.12 and 0.18 nm for S^{11+} and Cl^{12+} , respectively. In addition, the Zeeman split is symmetrically distributed; it has almost no impact on the line centroid determination. Therefore, the Zeeman effect can be safely neglected. The temperature in the laboratory was very stable and kept at 20 ± 0.5 °C, which reduces the time-varying expansion caused by temperature fluctuations. As a result, the thermal drift and mechanical drift could be neglected. In order to test the reliability of the uncertainty estimation, the wavelengths of three lines from highly charged argon ions were measured in the air, i.e., Ar^{9+} 553.3259(28) nm, Ar^{10+} 691.6864(28) nm, and Ar^{13+} 441.2567(26) nm, which were consistent with previously measured values of 553.3265(2), 691.6878(12), and 441.255919(6) nm [4,32], respectively.

Total uncertainties of measurement wavelength. Table III lists the synthesis of the uncertainties of S^{11+} and Cl^{12+} transition wavelength measurements. The total uncertainties were calculated from the root sum of the squares of the line centroid uncertainty and the dispersion function uncertainty, which was then combined linearly with the systematic uncertainties due to the wavelengths of the calibration lines, and due to the nonequivalence of the light distributions from the EBIT and the calibration lamps. Finally, the $M1$ transition wavelengths were determined to be 760.9635(29) and 574.1539(26) nm for S^{11+} and Cl^{12+} , respectively (in air). Improvements in the calibration and data treatment have enabled an order of magnitude improvement in precision compared to the previous visible spectroscopy at the SH-HtscEBIT [60].

In Table IV, we list the experimental and theoretical values for the ground state fine-structure splitting of boronlike S^{11+} . Fawcett *et al.* [9] did an experimental measurement in a chorine plasma generated in a 30-kJ, 37-kV θ -pinch device, and the uncertainty of the measured $M1$ transition of S^{11+} ion reaches 10^{-3} . The transition wavelength data of boronlike S^{11+} ions mainly come from the experimental data in the astronomical observation by Edlén in 1983. It can be seen from Table IV that Edlén's [26] astronomical observations and Jefferies [61] provide some deviations in the transition values, which are different from the results of our experimental measurements. In the theoretical calculation, the calculated results of Koc [62] in 2009 and Curtis *et al.* [63] in 1982 are generally consistent with the present calculation. The uncertainty of transition energy given by Yu's calculation is considerable [24]. Overall, most theoretical values do not have errors bars, which hampers the comparison.

TABLE IV. Comparison of the experimental and theoretical results of the fine structure in boronlike S^{11+} .

Year	Type	Energy (eV)	Wavelength (nm) (in air)	Ref.
2021	Expt. ^a	1.6288 60(6)	760.9635(29)	
1983	Expt. ^b	1.6285(1)	761.12(5)	[26]
1971	Expt.	1.637(13)	757.6(58)	[9]
1969	Expt. ^b	1.629 01(9)	760.881(43)	[61]
2021	Theor. ^c	1.6289(4)	760.93(19)	
2021	Theor.	1.6325	759.49	[34]
2019	Theor.	1.626(28)	762.7(13)	[24]
2018	Theor.	1.6332	758.93	[66]
2012	Theor.	1.6355	757.86	[33]
2011	Theor.	1.612	768.88	[67]
2009	Theor.	1.629 20	760.792	[62]
2003	Theor.	1.626 92	761.86	[65]
1996	Theor.	1.6303	760.28	[68]
1995	Theor.	1.6026	773.42	[69]
1982	Theor.	1.6289	760.93	[63]

^aExperimental measurement of this work.

^bObtained from Astronomical observation.

^cTheoretical calculations of this work.

Table V provides a comparison of the experimental and theoretical results of boronlike Cl^{12+} ions in recent years. Before our experiment, Fawcett *et al.* [9] measured the $M1$ transition of boronlike Cl^{12+} in the laboratory in 1971. Later on, the observed value was provided by Edlén [26] in 1983. The accuracies of the experimental results from Fawcett *et al.* [9] and the observed value of Edlén [26] both reached 10^{-3} . Thus, it can be found that our experimental measurement has improved the accuracy by two orders of magnitude. The theoretical calculation results of Curtis *et al.* [63], Edlén [26,64], Koc [62,65], and Artemyev *et al.* [19] are generally close to our experimental result. Our theoretical value, 2.1589(4) eV,

TABLE V. Comparison of the experimental and theoretical results of the fine structure in boronlike Cl^{12+} .

Year	Type	Energy (eV)	Wavelength (nm) (in air)	Ref.
2021	Expt. ^a	2.158 835(10)	574.1539(26)	
1983	Expt. ^b	2.1583(25)	574.29(67)	[26]
1971	Expt.	2.156 (7)	574.9(17)	[9]
2021	Theor. ^c	2.1589(4)	574.13(11)	
2021	Theor.	2.17036	571.26	[34]
2019	Theor.	2.153(35)	575.7(94)	[24]
2013	Theor.	2.1593(4)	574.02(11)	[19]
2012	Theor.	2.1655	572.54	[33]
2009	Theor.	2.159 32	574.016	[62]
2003	Theor.	2.155 59	575.008	[65]
1996	Theor.	2.1604	573.73	[68]
1995	Theor.	2.1238	583.61	[69]
1982	Theor.	2.1586	574.29	[64]
1982	Theor.	2.1592	574.21	[63]
1982	Theor.	2.1573	574.55	[11]

^aExperimental measurement of this work.

^bObtained from Astronomical observation.

^cTheoretical calculations of this work.

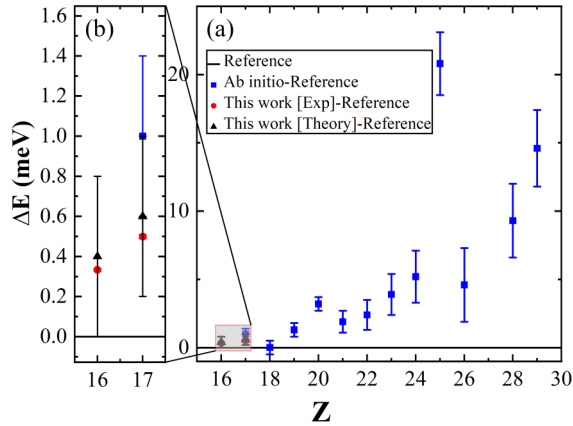


FIG. 5. (a) Comparison of the calculated results of boronlike ion *ab initio* for $16 \leq Z \leq 29$ and the experimental measurement results. It should be noted that the reference experimental values come from Edlén [26], the experimental value of $Z = 18$ is replaced by Draganić *et al.* [4], and the theoretical values come from *ab initio* reference Artemyev *et al.* [19]. (b) Enlarged view for detailed comparison of $Z = 16, 17$.

perfectly agrees with our experimental result, 2.158 826(10) eV.

Figure 5 shows the transition energy difference (ΔE) between the experimental values (reference Edlén [26]) and the present experimental measurement from this work of the boronlike ion ($16 \leq Z \leq 29$) and the theoretical result calculated by Artemyev *et al.* [19] with the *ab initio* method. The $Z = 16$ and $Z = 17$ sections are enlarged to provide more details. As can be seen from Fig. 5, the accuracy of the experiment is far ahead of theory in the region of Z around 18 and an agreement has been found between the theory and experiment. However, the differences between the experiment and theory become larger and larger with the increasing atomic number Z . Therefore, significantly more precise experiments than the existing measurements of highly charged B-like ions with $Z \geq 20$ would be interesting to test the previous experimental results as well as the theory of Artemyev *et al.* [19].

V. CONCLUSIONS

In conclusion, we present the experimental values for the wavelength measurements of the ground state $2s^2 2p^2 P_{1/2} - 2P_{3/2}$ transition of S^{11+} and Cl^{12+} , as well as the theoretically calculated values for the transition energy. The experimentally determined $M1$ transition wavelengths for S^{11+} and Cl^{12+} are 760.9635(29) and 574.1539(26) nm (in air), respectively. The $M1$ transition energies in S^{11+} and Cl^{12+} were also theoretically evaluated within the *ab initio* QED framework to compare with the experimental data. The present experimental results agree with the theoretical calculations. Compared to the previously observed values, the accuracies of current experimental results are improved by more than ten times and 200 times for S^{11+} and Cl^{12+} , respectively. To our knowledge, this work is the most accurate experimental measurement of S^{11+} and Cl^{12+} ions reported in the spectral range to date.

For fine-structure splitting $1s^2 2s^2 2p^2 P_{1/2} - 2P_{3/2}$ in boronlike isoelectronic ions, the accuracy of the experiment is far ahead of theory in the region of Z around 20, especially for $Z = 18$; an agreement has been found between the theory and experiment. However, there are almost no high precision measurements at higher $Z > 30$, therefore, significantly more precise experiments than the existing measurements of highly charged B-like ions would be interesting to test the theories.

ACKNOWLEDGMENTS

This work was partly supported by the National Key R&D Program of China under Grant No. 2017YFA0402300, the National Natural Science Foundation of China through Grants No. U1932207, No. 11904371, and No. 11974080, and Strategic Priority Research Program of Chinese Academy of Sciences Grant No. XDB34020000. W.Q.W. acknowledges the support from the Youth Innovation Promotion Association of the Chinese Academy of Sciences. A.V.V. was supported by the Government of the Russian Federation through the ITMO Fellowship and Professorship Program.

- [1] L. Malinovsky and M. Heroux, *Astrophys. J.* **181**, 1009 (1973).
- [2] L. Acton, M. Bruner, W. Brown, B. Fawcett, W. Schweizer, and R. Speer, *Astrophys. J.* **291**, 865 (1985).
- [3] E. Träbert, P. Beiersdorfer, S. Utter, G. Brown, H. Chen, C. Harris, P. Neill, D. Savin, and A. Smith, *Astrophys. J.* **541**, 506 (2000).
- [4] I. Draganić, J. C. López-Urrutia, R. DuBois, S. Fritzsche, V. Shabaev, R. S. Orts, I. Tupitsyn, Y. Zou, and J. Ullrich, *Phys. Rev. Lett.* **91**, 183001 (2003).
- [5] A. Artemyev, V. Shabaev, I. Tupitsyn, G. Plunien, and V. Yerokhin, *Phys. Rev. Lett.* **98**, 173004 (2007).
- [6] Y. S. Kozhedub, D. A. Glazov, A. N. Artemyev, N. S. Oreshkina, V. M. Shabaev, I. I. Tupitsyn, A. V. Volotka, and G. Plunien, *Phys. Rev. A* **76**, 012511 (2007).
- [7] H. S. Nataraj, B. K. Sahoo, B. P. Das, R. K. Chaudhuri, and D. Mukherjee, *J. Phys. B: At., Mol. Opt. Phys.* **40**, 3153 (2007).
- [8] J. Ullmann, Z. Anđelković, C. Brandau, A. Dax, W. Geithner, C. Geppert, C. Gorges, M. Hammen, V. Hannen, S. Kaufmann *et al.*, *Nat. Commun.* **8**, 15484 (2017).
- [9] B. C. Fawcett, A. H. Gabriel, and T. M. Paget, *J. Phys. B: At., Mol. Opt. Phys.* **4**, 986 (1971).
- [10] D. Flower and H. Nussbaumer, *Astron. Astrophys.* **45**, 349 (1975).
- [11] J. Sugar, V. Kaufman, and D. Cooper, *Phys. Scr.* **26**, 293 (1982).
- [12] M. Audard, E. Behar, M. Güdel, A. J. J. Raassen, D. Porquet, R. Mewe, C. R. Foley, and G. E. Bromage, *Astron. Astrophys.* **365**, L329 (2001).
- [13] W. Wang, X.-W. Liu, Y. Zhang, and M. Barlow, *Astron. Astrophys.* **427**, 873 (2004).
- [14] E. Träbert, G. Gwinner, A. Wolf, X. Tordoir, and A. G. Calamai, *Phys. Lett. A* **264**, 311 (1999).
- [15] E. Träbert, P. Beiersdorfer, G. V. Brown, H. Chen, E. H. Pinnington, and D. B. Thorn, *Phys. Rev. A* **64**, 034501 (2001).

- [16] E. Träbert, P. Beiersdorfer, G. Gwinner, E. H. Pinnington, and A. Wolf, *Nucl. Instrum. Methods Phys. Res., Sect. B* **205**, 83 (2003).
- [17] A. Lapiere, U. D. Jentschura, J. R. Crespo López-Urrutia, J. Braun, G. Brenner, H. Bruhns, D. Fischer, A. J. González Martínez, Z. Harman, W. R. Johnson *et al.*, *Phys. Rev. Lett.* **95**, 183001 (2005).
- [18] A. Volotka, D. Glazov, G. Plunien, V. Shabaev, and I. Tupitsyn, *Eur. Phys. J. D* **38**, 293 (2006).
- [19] A. N. Artemyev, V. M. Shabaev, I. I. Tupitsyn, and G. Plunien, *Phys. Rev. A* **88**, 032518 (2013).
- [20] M. Bilal, A. V. Volotka, R. Beerwerth, and S. Fritzsche, *Phys. Rev. A* **97**, 052506 (2018).
- [21] V. Yudin, A. Taichenachev, and A. Derevianko, *Phys. Rev. Lett.* **113**, 233003 (2014).
- [22] L. Schmöger, O. O. Versolato, M. Schwarz, M. Kohnen, A. Windberger, B. Piest, S. Feuchtenbeiner, J. Pedregosa-Gutierrez, T. Leopold, P. Micke *et al.*, *Science* **347**, 1233 (2015).
- [23] M. G. Kozlov, M. S. Safronova, J. R. Crespo López-Urrutia, and P. O. Schmidt, *Rev. Mod. Phys.* **90**, 045005 (2018).
- [24] Y. M. Yu and B. K. Sahoo, *Phys. Rev. A* **99**, 022513 (2019).
- [25] P. Micke, T. Leopold, S. A. King, E. Benkler, L. J. Spieß, L. Schmöger, M. Schwarz, J. R. Crespo López-Urrutia, and P. O. Schmidt, *Nature (London)* **578**, 60 (2020).
- [26] B. Edlén, *Phys. Scr.* **28**, 483 (1983).
- [27] D. J. Bieber, H. S. Margolis, P. K. Oxley, and J. D. Silver, *Phys. Scr.* **T73**, 64 (1997).
- [28] E. Trabert, P. Beiersdorfer, G. Gwinner, E. H. Pinnington, and A. Wolf, *Phys. Rev. A* **66**, 052507 (2002).
- [29] R. S. Orts, Z. Harman, J. R. C. López-Urrutia, A. N. Artemyev, H. Bruhns, A. J. G. Martínez, U. D. Jentschura, C. H. Keitel, A. Lapiere, V. Mironov *et al.*, *Phys. Rev. Lett.* **97**, 103002 (2006).
- [30] A. Lapiere, J. R. C. López-Urrutia, J. Braun, G. Brenner, H. Bruhns, D. Fischer, A. J. G. Martínez, C. O. V. Mironov, G. Sikler, R. S. Orts *et al.*, *Phys. Rev. A* **73**, 052507 (2006).
- [31] V. Mäckel, R. Klawitter, G. Brenner, J. R. C. Lopez-Urrutia, and J. Ullrich, *Phys. Rev. Lett.* **107**, 143002 (2011).
- [32] A. Egl, I. Arapoglou, M. Höcker, K. König, T. Ratajczyk, T. Sailer, B. Tu, A. Weigel, K. Blaum, W. Nörtershäuser *et al.*, *Phys. Rev. Lett.* **123**, 123001 (2019).
- [33] J. P. Marques, P. Indelicato, and F. Parente, *Eur. Phys. J. D* **66**, 324 (2012).
- [34] L. Natarajan, *Phys. Scr.* **96**, 105402 (2021).
- [35] J. Xiao, R. Zhao, X. Jin, B. Tu, Y. Yang, D. Lu, R. Hutton, and Y. Zou, in *Proceedings of the 4th International Particle Accelerator Conference, IPAC2013 (JACoW, Shanghai, China, 2013)*, pp. 434–436.
- [36] B. Tu, Q. Lu, T. Cheng, M. Li, Y. Yang, K. Yao, Y. Shen, D. Lu, J. Xiao, and R. Hutton, *Phys. Plasmas* **24**, 103507 (2017).
- [37] W. Li, S. Zhan, Y. Yang, J. Xiao, and Y. Zou, *Phys. Rev. A* **91**, 062501 (2015).
- [38] Q. Lu, J. He, H. Tian, M. Li, Y. Yang, K. Yao, C. Chen, J. Xiao, J. G. Li, and B. Tu, *Phys. Rev. A* **99**, 042510 (2019).
- [39] S. Y. Liang, T. X. Zhang, H. Guan, Q. F. Lu, J. Xiao, S. L. Chen, Y. Huang, Y. H. Zhang, C. B. Li, Y. M. Zou *et al.*, *Phys. Rev. A* **103**, 022804 (2021).
- [40] A. Kramida, Yu. Ralchenko, J. Reader, and N. A. Team, NIST Atomic Spectra Database, Ver. 5.8.
- [41] <https://physics.nist.gov/PhysRefData/ASD/Html/lineshelp.html#AIR>
- [42] A. V. Malyshev, D. A. Glazov, A. V. Volotka, I. I. Tupitsyn, V. M. Shabaev, G. Plunien, and T. Stöhlker, *Phys. Rev. A* **96**, 022512 (2017).
- [43] A. V. Malyshev, D. A. Glazov, A. V. Volotka, I. I. Tupitsyn, V. M. Shabaev, and G. Plunien, *Nucl. Instrum. Methods Phys. Res., Sect. B* **408**, 103 (2017).
- [44] P. J. Mohr, G. Plunien, and G. Soff, *Phys. Rep.* **293**, 227 (1998).
- [45] V. M. Shabaev, *Phys. Rep.* **356**, 119 (2001).
- [46] Y. S. Kozhedub, A. V. Volotka, A. N. Artemyev, D. A. Glazov, G. Plunien, V. M. Shabaev, I. I. Tupitsyn, and T. Stöhlker, *Phys. Rev. A* **81**, 042513 (2010).
- [47] A. V. Malyshev, A. V. Volotka, D. Glazov, I. I. Tupitsyn, V. M. Shabaev, and G. Plunien, *Phys. Rev. A* **90**, 062517 (2014).
- [48] A. V. Malyshev, A. V. Volotka, D. A. Glazov, I. I. Tupitsyn, V. M. Shabaev, and G. Plunien, *Phys. Rev. A* **92**, 012514 (2015).
- [49] A. V. Volotka, M. Bilal, R. Beerwerth, X. Ma, T. Stöhlker, and S. Fritzsche, *Phys. Rev. A* **100**, 010502 (2019).
- [50] V. M. Shabaev, I. I. Tupitsyn, and V. A. Yerokhin, *Phys. Rev. A* **88**, 012513 (2013).
- [51] V. A. Yerokhin and V. M. Shabaev, *J. Phys. Chem. Ref. Data* **44**, 033103 (2015).
- [52] I. I. Tupitsyn, V. M. Shabaev, J. C. López-Urrutia, I. Draganić, R. S. Orts, and J. Ullrich, *Phys. Rev. A* **68**, 022511 (2003).
- [53] I. I. Tupitsyn, A. V. Volotka, D. A. Glazov, V. M. Shabaev, G. Plunien, J. R. Crespo López-Urrutia, A. Lapiere, and J. Ullrich, *Phys. Rev. A* **72**, 062503 (2005).
- [54] M. Y. Kaygorodov, Y. S. Kozhedub, I. I. Tupitsyn, A. V. Malyshev, D. A. Glazov, G. Plunien, and V. M. Shabaev, *Phys. Rev. A* **99**, 032505 (2019).
- [55] R. N. Faustov, *Theor. Math. Phys.* **3**, 478 (1970).
- [56] J. Sucher, *Phys. Rev. A* **22**, 348 (1980).
- [57] N. A. Zubova, Y. S. Kozhedub, V. M. Shabaev, I. I. Tupitsyn, and T. Stöhlker, *Phys. Rev. A* **90**, 062512 (2014).
- [58] N. A. Zubova, A. V. Malyshev, I. I. Tupitsyn, V. M. Shabaev, Y. S. Kozhedub, G. Plunien, C. Brandau, and T. Stöhlker, *Phys. Rev. A* **93**, 052502 (2016).
- [59] N. Kimura, R. Kodama, K. Suzuki, S. Oishi, M. Wada, K. Okada, N. Ohmae, H. Katori, and N. Nakamura, *Phys. Rev. A* **100**, 052508 (2019).
- [60] Q. Lu, C. L. Yan, G. Q. Xu, N. Fu, Y. Yang, Y. Zou, A. V. Volotka, J. Xiao, N. Nakamura, and R. Hutton, *Phys. Rev. A* **102**, 042817 (2020).
- [61] J. T. Jefferies, *Mem. Soc. R. Sci. Liege* **15**, 213 (1969).
- [62] K. Koc, *Eur. Phys. J. D* **53**, 9 (2009).
- [63] L. J. Curtis and P. S. Ramanujam, *Phys. Rev. A* **26**, 3672 (1982).
- [64] B. Edlén, *Phys. Scr.* **26**, 71 (1982).
- [65] K. Koc, *J. Phys. B: At., Mol. Opt. Phys.* **36**, L93 (2003).
- [66] W. Kai, S. C. Xian, J. Per, E. Jörgen, G. Michel, Z. C. Yu, S. Ran, Z. X. Hui, C. C. Yang, and Y. Jun, *Astrophys. J.* **864**, 127 (2018).
- [67] G. Y. Liang, N. R. Badnell, G. Zhao, J. Y. Zhong, and F. L. Wang, *Astron. Astrophys.* **533**, A87 (2011).
- [68] M. S. Safronova, W. R. Johnson, and U. I. Safronova, *Phys. Rev. A* **54**, 2850 (1996).
- [69] G. Merkelis, M. J. Vilkas, G. Gaigalas, and R. Kisielius, *Phys. Scr.* **51**, 233 (1995).